Journal of Petroleum Science and Engineering 173 (2019) 222–236

Contents lists available at ScienceDirect

Journal of Petroleum Science and Engineering

journal homepage: www.elsevier.com/locate/petrol

Flow modelling of unconventional shale reservoirs using a DFM-MINC proximity function

N. Farah[a,b,*], M. Delorme[a], D.Y. Ding[a], Y.S. Wu[c], D. Bossie Codreanu[a]

[a] IFP Energies Nouvelles, 1 & 4 Avenue Bois Préau, Rueil-Malmaison, 92852, France
[b] Lebanese American University, P.O. Box 36, Blat, Byblos, Lebanon
[c] Colorado School of Mines, 1500 Illinois St, Golden, CO, 80401, USA

A R T I C L E I N F O

Keywords:
Fractured reservoirs
Unconventional reservoirs
Fracture-matrix interaction
Shale-gas
Tight-oil
DFM-MINC proximity function

A B S T R A C T

Due to their initial low permeability, unconventional plays can be economical only through hydraulic fracturing. This process, in order to be controlled needs to rely on a solid representation of the natural fracture geometry, an accurate stimulation model which considers the interaction with natural lineaments, and a physical reservoir model which can account for the different flow regimes occurring during production. The stimulated volume drainage can be evaluated using either Decline Curves Analysis/Rate Transient Analysis (DCA/RTA) techniques or reservoir simulation. In both cases, the geometry of the final Discrete Fracture Network (DFN) issued from the natural characterization and the stimulation, is very important, and for practical purposes is either overly idealized (Warren & Root approach) or oversimplified (Bi-wing). The models have shown their limitations when confronted with measurements in the field, opening up ways to use DFN geometries within integrated reservoir studies.

The present work addresses some of the issues above, developing a hierarchical Discrete Fracture Model (DFM) based on the “filtering” of a stimulated DFN, realistically obtained by the characterization step and the stimulation process. This leads to a triple-continuum representation, consisting of: (1) the matrix media, (2) a high conductive stimulated fracture network and (3) a low conductive stimulated fracture network.

The method consists in homogenizing low conductive networks, keeping a user defined backbone of high conductive fractures as the main “reservoir” DFN. One of the main advantages of this DFM relies on the way we compute the well-known Multiple Interacting Continua (MINC) approach, using a “proximity function” formalism, able to simulate transient effects. Using practical examples, this paper demonstrates applicability capacities of this method, enabling the integration of more complex geometries within a “quick” simulation framework.

1. Introduction and industrial issues

1.1. Issues and definition

Unconventional shale/tight reservoirs, holding a significant amount of the world's hydrocarbon reserves, present very low permeability characteristics, rendering their production possible only through multi-stage hydraulic fracturing by maximizing the Stimulated Reservoir Volume (SRV), where; the hydraulic fracturing is an effective technique to enhance productivity, with a great impact on the performance of a fractured well (Ozkan et al. (2011)). Note that, the SRV accounts for the volume of porous media where complex network distribution formed from naturally induced fractures, multiple hydraulic fractures, and original matrix; where it is characterized by an induced matrix permeability which is typically greater (or equal, case dependant) than the original matrix permeability (Al-Rbeawi (2017, 2018)). Moreover, such reservoirs are often naturally fractured, showing non percolating complex natural fracture geometries. Their distribution might be non-stationary, difficult to characterize (orientation lengths and densities), thus making systematic homogenization dangerous.

Studies of the hydraulic fracturing process use either reservoir DCA (Decline Curve Analysis), PTA (Pressure Transient Analysis)/RTA (Rate-transient analysis) or simulation models. The routinely used DCA methods adapted for unconventional reservoirs (Stretched Exponential Model, Duong Model, power law exponential, logistic growth decline …) follow fundamental work originally established by Arps (1945). RTA is based on the same physics governing fluid storage and flow as for PTA. In other words, RTA uses well flowing well pressures along

* Corresponding author. Lebanese American University, P.O. Box 36, Blat, Byblos, Lebanon.
E-mail address: nicolas.farah@lau.edu.lb (N. Farah).

https://doi.org/10.1016/j.petrol.2018.10.014
Received 19 February 2018; Received in revised form 21 September 2018; Accepted 6 October 2018
Available online 10 October 2018

with production rates to extract information. They rely on curve fitting of historical production data, followed by projection forecasts. Specific unconventional reservoir mechanisms; such as non-static permeability, complex fracture networks, non-Darcy flow, adsorption etc.; were added in additional models improving characterization of multiple fractured horizontal wells at different stages of their life (Ketineni and Ertekin (2012), Stalgorova and Mattar (2013)). In particular, the linear rate signal exhibited from online early-time production data, if macroscopic reservoir and fluid properties are known, is analyzed, leading to total effective fracture area estimation. Although analytical production data analysis methods analyses are routinely used for conventional reservoirs, complexities associated to unconventional reservoirs make their use delicate. All assume a priori geometries governing hydraulic fracturing, leading to improved formulations, all addressing specific characteristics and operational conditions (summarized in Okouma Mangha et al. (2012)), integrating the role fractures play (hydraulically stimulated). Moreover, these methods are data intensive if reliable forecast are expected. Ideally, they should be used in parallel with numerical methods, thus constraining decline-curve forecast. Workflows to ensure this consistency have been provided in the literature for all reservoir types (Fetkovich et al. (1996); Mattar and Anderson (2003), Clarkson (2013)).

Therefore, historical "engineered" representations such as Bi-Wing approaches (Nordgren (1972), Daneshy (1973), Barree (1983), Bouteca (1988)) or wiremesh (Xu et al. (2010), Weng et al. (2011), Meyer and Bazan (2011)) became widely used. These model theoretically work well when reservoir characteristics within the stimulated areas, such as natural fractures, are known to be stationary and isotropic, leading to homogenization, and therefore to one main stimulation path, (Parsegov et al., 2018). Yet, hydraulic fracturing monitoring data such as microseismic or tomographic techniques have determined that fracture paths interact, between induced and natural fractures, creating more complex geometries. Other methods such as Production Logging Tools (PLT) or Data Acquisition System (DAS) confirmed the above phenomena, spatially not matching the same locations probably due to tools investigation resolution. Most recently, the Eagle Ford in-situ information project Hydraulic Fracture Test Site (HFTS), using various data acquisition methods, has shown the complex nature of such networks and the lack of predictability of "classical" approaches (Raterman et al. (2017)). Even when natural fractures are scarce, the developed geometry can become quite complex, consisting in many fracture branches making up active clusters (Delorme et al. (2016), see; Fig. 1). Due to properties of stimulation fluids, multi-scale geometries develop, potentially complex, according to specific boundaries connecting the well to the reservoir volume. That way different zones of the reservoir are enhanced, thus affecting overall gas or/and oil production (Huang et al. (2014)). In conclusion, the heterogeneity and the complexity of the reservoir become dynamic properties, making flow modelling from such reservoirs quite challenging for both stimulation and production simulation.

Discrete Fracture Network (DFN) characterization techniques have been used to describe unconventional reservoirs, simulating stimulation processes leading to complex fracture geometries. Several modelling approaches can be cited, enabling comparison or calibration using microseismic (Mayerhofer et al. (2006), Williams-Stroud (2008)), or pressure data (Elmo and Stead (2010), Nagel et al. (2013), McClure et al. (2015)), or both (Delorme et al. (2013)). Historically, the difficulties in applying these approaches concern the CPU intensive needs, in order to be able to account for potentially a large amount of fractures, and the reservoir property uncertainty through sensitivity simulations. The present approach addresses this problem, solving the CPU handicap, while retaining part of the initial complexity. Particular effort is done to capture principal heterogeneities as well as transient behavior, using an adequate mesh. This leads to a main "backbone" network, interacting through an adequately refined tight matrix which favors nonlinear fracture matrix exchange terms often important in such plays. This effect is well described in Yan et al. (2016b), who has evaluated various shape factors used in dual porosity models, giving examples highlighting the necessity of intra-porosity transfer terms refinement to accurately restitute transients. Recently, Fuentes-Cruz et al. (2014) presented a model for transient behavior of shale gas. Fuentes-Cruz et al. (2014) modeled three cases of permeability variation: uniform (with no variation in permeability), linear and exponential; were they used type-curve matching for the identification of the appropriate permeability model type. A linear flow followed by a pseudosteady-state regime was naturally found for the uniform model case. This obviously makes a good case, implying that realistic field permeabilities will cause a deviation from the linear flow. Founding the realistic shape factor becomes mandatory.

1.2. Theoretical prerequisite

The general equation governing three-phase, three-dimensional flow in naturally fractured reservoirs for a single porosity model using different petro-physical properties for matrix and fractures media, is written as follows. The general form of the diffusivity equation in any coordinate system, arbitrary spatial dimensions, heterogeneous permeability/viscosity, including gravity can be written as:

$$\nabla.\left[\frac{\mathrm{K}k_{rp}}{\mu_p B_p}\nabla(P+\rho g z)\right]=\frac{\varnothing c_t}{B_p}\frac{\partial P}{\partial t}-\tilde{q}_p^{sc} \tag{1}$$

where, the subscript p represents the phase, K is the absolute

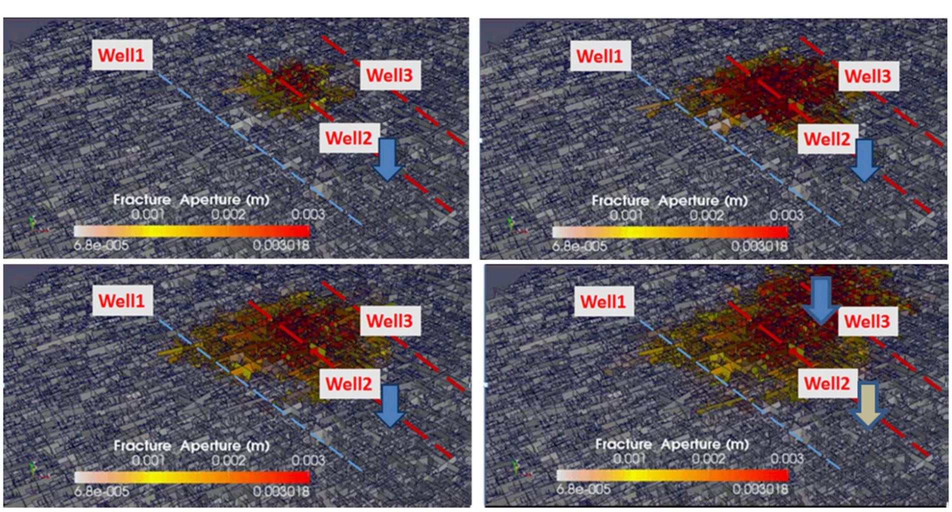

Fig. 1. A large fracture network, and conductivity distribution, with an irregular fractures distribution intersecting with (several) horizontal well at different injection times: (a) slick water injection (30min in well 2), (b) proppant injection in Well 2 (70min), (c) slick water injection in Well 3 (210 min) (d) proppant injection in well 2 (230 min) (after; Delorme personal communication).

permeability tensor of the medium, k_{rp} is the relative permeability of phase p, μ_p is the viscosity of phase p, B_p is the volumetric factor of phase p, P is the pressure of phase p, ρ is the density, g is the algebraic value of gravitational acceleration projection on z axis, z is depth (positive, increasing downwards), $\varnothing$ corresponds to the porosity, c_t is the total compressibility. Also, $\tilde{q}_p^{sc}$ is the sink/source term of phase p.Where the total compressibility, c_t, is defined as the sum of the rock compressibility (c_r) and the fluid compressibility (c_f):

$$c_t = c_r + c_f \tag{2}$$

1.3. Setting up the problem

To model a realistic reservoir fracture network, a single-porosity model where fractures are explicitly discretized is intellectually appealing. However, such approach leads to simulations consuming large computational CPU time due to the large number of grid cells needed, when matrix and fracture cells need to be conforming. On the other hand, dual-porosity model, are often inadequate for such problems due to the single averaged unknown describing potentially large matrix grid-blocks for which the pseudo-steady state hypothesis is probably wrong for extremely low matrix permeability reservoirs (Moinfar et al. (2011), Kuchuk and Biryukov (2014), Jiang and Younis (2016)). Furthermore, during the transient period in shale-gas reservoirs, a non-linear variation of the pressure in the matrix media increases the duration of the transient effects leading to a long transient periods which cannot be handled by dual-continuum models (Chai et al., 2016), Yan et al. (2016a). However, note that dual-porosity model is still largely used providing solution under specific assumptions such as “smooth special heterogeneity and short transients”. Moreover, dealing with gas formation in a three phase reservoir conditions, even if the error might be small, Gas Oil Ratio might be badly predicted as the pressure gradient within the matrix grid-block is coarsely accounted for (Delorme et al., 2017).

That’s why lately, the basis of a new developments rely on the type model called Discrete Fracture Model (DFM) has been largely studied (Sarda et al. (2002), Karimi-Fard et al. (2004, 2006), Pichot et al. (2012), Norbeck et al. (2014), Ngo et al. (2017). These models rely on unstructured grids to conform to fracture geometry and locations, where all fracture types are explicitly discretized, potentially leading to a complicated (in 3D) and difficult to tract numerical system to solve (Sun and Schechter (2015)). Furthermore, even if these were to be known, to our knowledge there is no numerical solution which is able to handle up to 300,000 fractures. To overcome these limitations, Lee et al. (2001), Moinfar et al. (2013), Norbeck et al. (2014) propose a hierarchical method, dealing more easily with these problems using length criteria to limit the number of fractures to be accounted for. Khvoenkova and Delorme (2011) presented a DFM with a reduced number of degree of freedom thanks a tailored numerical scheme (one node at each intersection only being required) enabling to deal with a larger number of fractures. This model, suited for several wells scale studies aim to capture the dynamic behavior of fractured reservoir systems in which both the properties of individual fractures and the connectivity of fracture networks are expected to evolve over time (Delorme et al. (2013, 2016)). Moreover, the matrix-fracture interaction is difficult to handle within these approaches because of the very low matrix permeability that imply very fine gridding in the matrix media. See for example (Artus and Fructus (2012), Sun et al. (2016)) and all literature on the widely applied logarithmically spaced/locally refined (LS/LR) DFM technique. Non-conforming meshing strategies have therefore been developed; (Reichenberger et al. (2006), Khvoenkova and Delorme (2013), Fumagalli and Scotti (2013), Berrone et al. (2014)).

Recently, Yan et al. (2017) and Mi et al. (2017) presented an Enhanced Discrete Fracture Network (EDFN) model for multiphase flow simulation in fractured reservoirs. EDFN is based on Voronoï technique in order to discretize the matrix domain (DFN + image processing; see also Sarda et al. (2002) in 2D, and Delorme (2015)) coupled with the standard MINC method where, the fracture network is discretized by assigning fracture nodes to each fracture intersecting points and fracture extremities. Note that, the EDFN approach refines (subdivides) the matrix grid block using a Local Grid refinement (LGR) technique in the direction perpendicular to the fracture surface (1D MINC method).

In fact, the main difference between our proposed approach and similar approaches presented in the literature relies on the application of the MINC method. For example, the EDFN proposed by Yan et al. discretizes logarithmically the equivalent matrix grid blocks using a 1D MINC method to handle the flow between the matrix and the fracture, when in this proposed approach the MINC exchange terms are estimated during the image processing of the proximity function by applying a method introduced by Delorme (2015). Using a MINC proximity function (detailed in part 2), our proposed model ensures a well modelling of the matrix-fracture flow interaction by subdividing the matrix domain into nested volume taking into account the modeled matrix-fracture distance distribution. This is not the case in the above references where the influence volume only seems to be estimated using the Voronoï technique.

More generally, this model can be considered of the same family of Akkutlu et al. (2017) proposing a practical methodology to address this issue by combining efforts in reducing the number of unknowns to describe both the fracture and the matrix media while describing adequately long transient effects. The difference with Akkutlu et al. relies in the fact that in our case, fine scale simulation at the grid block scale are not necessary to estimate boundary conditions, they are assumed.

1.4. Method outline

Fractured reservoirs are complex (Fig. 1), heterogeneous and anisotropy. If they are to be treated mathematically, certain idealizations must be taken into consideration (are imperative) especially under practical considerations such as a rock matrix with very low permeability compared with fractures. The United States Geological Survey (USGS) has set a standard, such as “a reservoir with permeability less than 0.1 mD” as being considered as a tight reservoir. Under these circumstances, modelling the flow from such reservoirs with a standard dual-porosity (DP) model becomes very challenging since by definition it always assumes pseudo steady-state within the matrix.

Also, the presence of natural fractures affects the flow, since their interaction with hydraulically induced fractures can guide the development of an effective SRV. This implies knowing precisely the heterogeneity nature of many properties of the formation, which becomes also a real challenge. The main objective of this work is to propose a new DFM to deal quickly but adequately with this kind of heterogeneity often seen in tight reservoirs and to model correctly the flow exchange between the matrix and the different existing fractures, extending the MINC matrix-fracture flow exchanges formulation, attempting to be able to simultaneously account better for the transient period and keep a tractable number of unknowns. To do so, we propose a DFM-MINC proximity function in order to model flow from low reservoir permeability.

In our proposed approach, the DFM is coupled with two other media: (1) the matrix media zone and (2) a low conductive homogenized but connected fractures. The exchanges between these media mentioned above are modeled using the MINC formalism. As known, the MINC method was originally developed by Pruess and Karasaki (1982) (see also, Wu and Pruess (1988)) to model heat and multiphase fluid flow in fractured porous media. This concept consists in subdividing individual matrix blocks into several nested meshes which could result in a better modelling of the flow from matrix media towards the fractures. Note that, the main difference between the MINC method and a DP (dual-porosity) is based on how the pressure gradients are accounted for. The DP model simulates matrix-fracture exchange on

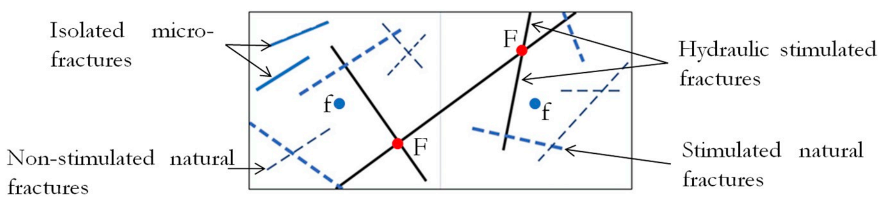

Fig. 2. Illustration of different fractures types occurring into a reservoir.

the basis of a pseudo-steady state flow hypothesis, whereas the MINC method treats the problem entirely by a numerical method creating fully the transients. Thus, in our new scheme, two exchanges occur: one between the matrix and a low conductivity homogenized zone and a second one between the fracture path (relating the reservoir to the wellbore) and the global zone made up of the matrix and the homogenized zone.

2. DFM based on a MINC proximity function

Unconventional reservoirs are naturally fractured with the presence of connected and isolated fractures. For an economic production, low permeability reservoirs are stimulated using hydraulic techniques, in a way to improve reservoir permeability by creating a stimulated fractures network connecting a huge reservoir volume to the wellbore.

Using horizontal well, creating several levels (scale dependent) of complexity, this can be classified as: hydraulically stimulated - induced fractures; interacting fractures (stimulated natural fractures + induced fractures); non-stimulated natural fractures and even micro-fractures within the organic matter (see; Fig. 2). All these types of fractures are connected to each other leading to a very complex potentially continuous DFN (fully continuous at least for the part relating the reservoir to the wellbore or partly continuous). A realistic representation of such a full network would require too many unknowns and could easily become a non-tractable numerical system.

Therefore, in order to simplify the system we have chosen to develop a three media approach which fully accounts transient effects. The main challenge of the method resides in adequately choosing spatial delineation of the three media and estimating correctly the exchange term functions between each media.

The DFM is coupled with a MINC proximity function based on the distance to all discrete fractures using a stochastic random point's distribution (Khvoenkova and Delorme (2013)). The proposed DFM-MINC proximity function is based on a triple continuum media taking into consideration: (1) matrix media, (2) homogenized fracture media and (3) highly conductive fractures which are explicitly discretized. Therefore the implemented MINC formalism applies to the majority of fracture types found in unconventional reservoirs. The idealization/approximation used is to consider two types of continuous fracture media: (a) highly conductive fractures and (b) a stimulated natural fractures with lower conductivities compared to hydraulic fractures. In other words, to treat the presence of multi-scale fractures we suggest classifying different existing fractures into the reservoir using a hierarchy based on a conductivity criterion combined with connectivity. Note that, the conductivity threshold between high and low fractures conductivity could be defined by the user.

Thus, high conductive fractures are explicitly discretized due to their crucial role in production, while other fractures are homogenized leading to a homogenized fracture media lightly permeable. Besides, our proposed DFM-MINC proximity function subdivides the matrix media using the MINC method and mesh-less approach to simulate properly the flow exchange between matrix and all sorts of fractures (including both high and low conductive fractures). Refinement inside the continuous media is flexible and user-defined. As an example of validation, Fig. 3 presents the Error (compared to reference solution) in L_2 norm function number of matrix refinement for the cumulative gas production; for both single and multiphase flow cases (see; Farah et al. (2016)).

Our approach is appropriate for describing a large reservoir since it treats the multi-scale problem. As mentioned above, three media exist into our proposed discrete fracture model; the matrix, the homogenized natural fractures (secondary) and hydraulic fractures (primary) denoted m, f and F; respectively. Note that, different connections between different media exist and are identified as follows; connection between primary and homogenized fracture (F-f), between homogenized fracture cells (f-f), between homogenized fracture and matrix (f-m) and finally between primary fracture and matrix (F-m). Moreover, the connection between primary fractures and matrix (F-m) are also considered via the MINC approach. In fact, the MINC proximity function is computed with respect to all the fractures, including primary fractures (F) and natural fractures (f). So, the matrix-fracture exchange in the MINC approach includes all fracture types. However, for the equivalent (homogenized) fracture permeability and porosity computation, only low conductive fractures are considered.

Thus, the proposed DFM consists in discretizing explicitly hydraulic and highly conductive fractures, due to their very important role during the production when other fractures are homogenized. Discretization is performed at each fracture plane intersection to which a fracture node is associated (represented by a red node in Fig. 2). Fractures porosity and surface exchange values are assigned to each fracture node. Furthermore, homogenized fractures are assigned using another representative node, which is represented by a blue node in Fig. 2. Finally, the matrix media is represented with a third node connecting with the homogenized fractures through the blue node. In the matrix media the MINC proximity function is applied taking into account all existing fracture types into the grid cell. For a deeper investigation on how the MINC proximity function is computed see, Farah (2016); Appendix A – MINC Proximity Function; where a detailed description of the MINC proximity function is presented.

For convenience, a MINCn model is defined as one matrix cell is subdivided into “n” nested volumes. (For example; a MINC6 means that the matrix media has been subdivided into 6 subdivisions). Moreover, in order to perform this kind of DFM, a homogenization method must be taken into account. To do so, a study comparing an analytical approach, a local numerical upscaling and a global numerical upscaling; in order to quantify the effect of the homogenization method on our DFM; is done (see; Khvoenkova and Delorme (2009); Farah (2016)). Note that, in this work the equivalent permeabilities are computed with a global numerical upscaling method on the homogenized fracture cells, as we found it was the most accurate homogenization method in this case.

Fig. 4 summarizes the several steps to apply in order to compute our DFM-MINC proximity function on an irregular complex discrete fracture network. It must be mentioned that, the matrix-fracture exchange is particularly important for low matrix permeability reservoirs, inducing long transient periods. Connections between different media and transmissibility calculations are described in details below.

2.1. Intersection between the well and the hydraulic fractures

A node (green node in Fig. 5) is assigned to the intersection between the well (red dashed line in Fig. 5) and the hydraulic fracture. Hence, a connection between the intersection of the horizontal well (green node in Fig. 5) and the hydraulic fracture node (red node in Fig. 5) is done

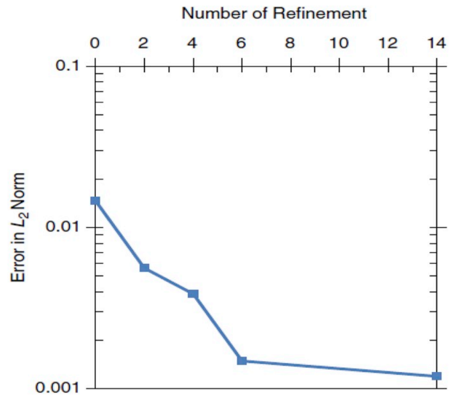

Fig. 3. The L_2 norm Error function of number of refinement concerning (left) a single-phase flow and (right) a multiphase flow for the cumulative gas production from a reservoir example (see; Farah et al. (2016)).

through the calculation of the transmissibility using Eq. (3).

$$T_{well-F} = \frac{k_F}{d_{well-F}} A_F \tag{3}$$

where, k_F is the fracture permeability, A_F corresponds to the exchange surface ($A_F = e_F * Z_F$) (note that, e_F and Z_F corresponds to the hydraulic fracture aperture and the fracture depth in z direction; respectively) and d_{well-F} correspond to the average distance between the two nodes (red and green nodes). To take into account the radial flow behavior towards the well, a numerical PI is used for the flow modelling inside the fracture plane to connect the calculated well node pressure and the true wellbore pressure. Note that, only an intersection of primary fractures network with a well are taken into consideration (green node is assigned; Fig. 5).

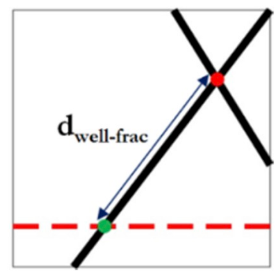

Fig. 5. Illustration of the intersection between a horizontal well and a hydraulic fracture.

2.2. Flow between hydraulic (primary) fractures

As stated above, the flow between highly conductive fractures should be taken into consideration and is explicitly discretized. Each "impacting" fracture is explicitly modeled, using a limit number of fractures nodes. Each intersection of two (or more) high conductive or hydraulic fractures is first computed. The fracture volumes and the exchange surfaces are assigned to the fracture nodes and are estimated using a Voronoï mesh in each fracture plane (see, Delorme et al. (2013)). Here, Fig. 6(a) presents an illustration of a 2D example consisting of; hydraulic, natural and isolated fractures, where each intersection between hydraulic fractures plane (solid black lines) is assigned with a fracture node (red node in Fig. 6(b)).

Due to the model choices, a connection between the fracture nodes F_i and F_j occurs along one fracture only, facilitating its computation via Eq. (4):

$$T_{F_i\,/\,F_j} = A_F * \frac{k_F}{d_{ij}} \; and \; A_F = e_F * l_{Fij} \tag{4}$$

where, k_F corresponds to the fracture permeability, A_F to the fracture exchange area and d_{ij} represents the distance between the two fracture nodes, respectively node i and j. Also, e_F corresponds to the hydraulic

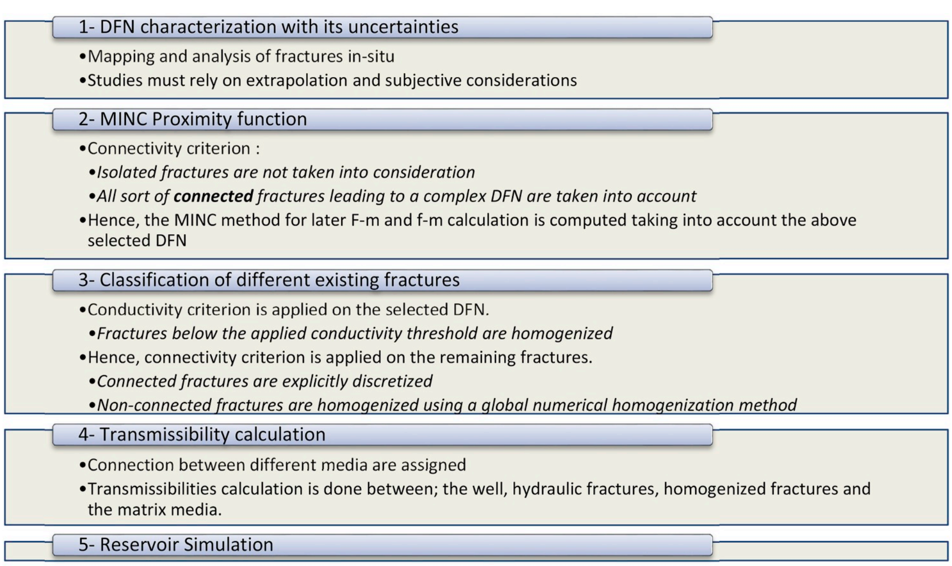

Fig. 4. The several steps to follow leading to the application of our proposed DFM on a complex fracture network.

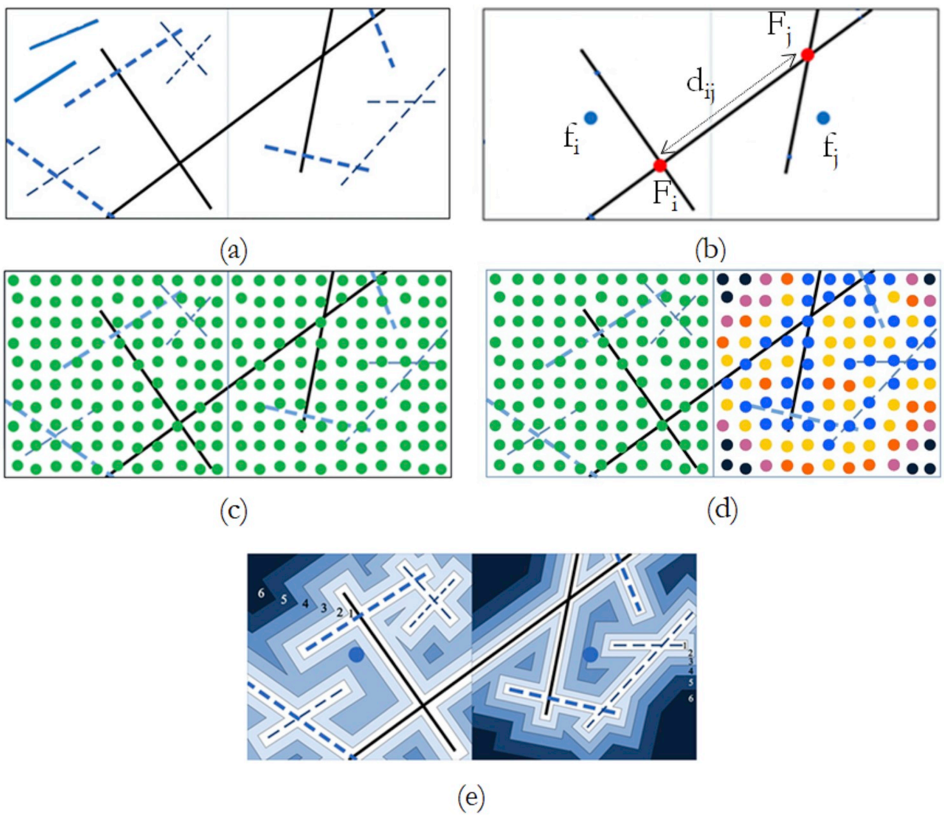

Fig. 6. Illustration of (a) an irregular DFN (b) principal hydraulic fractures intersecting with each other's (solid black lines) where a red node (F_i and F_j) is assigned to each hydraulic fracture intersection, (c) the random p points launched in each homogenized grid cell (f_i and f_j) intersecting with a hydraulic fracture, (d) the calculated distance of each point to the nearest fracture where different colors (blue, orange, grey, purple and black) represent different distances to the nearest fracture; blue (the nearest) and black (the farthest) and (e) DFM-MINC6 proximity function taking into account all sort of connected fractures. (For interpretation of the references to color in this figure legend, the reader is referred to the Web version of this article.)

fracture aperture and l_{Fij} corresponds to the borderline length between the cells (fracture depth in z direction in the 2D case, but requires Voronoï segment calculations inside the fracture in 3D to be K-orthogonal, Delorme et al. (2016)).

2.3. Exchange between primary fractures and homogenized fractures

To connect the primary fractures (red node F_i in Fig. 6(b)) to the homogenized media (blue node f_i in Fig. 6(b)), the transmissibility is calculated using Eq. (5):

$$T_{F_i/f_j} = \frac{k_{f_i}{*}k_{F_i}\,(d_{f_i} + d_{F_i})}{k_{f_i}{*}d_{F_i} + k_{F_i}{*}d_{f_i}} {*} \frac{A_{F_i}}{(d_{f_i} + d_{F_i})} \approx \frac{k_{f_i}}{d_{f_i}} {*} A_{F_i} \tag{5}$$

where, f_i corresponds to a homogenized fracture grid cell node, F_i corresponds to a hydraulic fracture node, A_{F_i} corresponds to the principal fracture exchange surface of node F_i within the homogenized grid cell f_i, k_{f_i} corresponds to the homogenized fractures permeability. The distance d_{f_i} corresponds to the average distance from the grid cell to the principal (hydraulic) fractures.

Note that, the average distance $<d_{f_i}>$ of a homogenized grid cell i to the fracture existing into a grid cell is calculated using the same stochastic approach based on a randomly method (randomly points distribution inside the studied grid cell). Firstly, the cell grid is discretized into n sub-domains, and then a point is randomly selected in each sub-domain (see, Fig. 6(c)). Using this method may avoid biased distance distribution computation for fractures of type Warren and Root, where the fractures are parallel to the grid axes. Moreover, it allows numerical problem simplification without requiring complicated meshing procedure that might be involved in workflows using the same ideas (Yang et al. (2017)).

The average distance d_n of a homogenized grid cell to the hydraulic fractures is obtained.

$$<d_{f_i}> = \frac{1}{n}\sum_{p=0}^{n-1} d_{p(pt-frac)}$$

where, n is the number of sample points launched into the studied grid cell and $d_{p(pt-frac)}$ corresponds to the distance from each sample point to the nearest fracture inside the grid cell.

2.4. Flow between homogenized low conductive fractures

The connection between two grid cells of homogenized low conductivity fractures, identified by a blue node in Fig. 6(b), is calculated using Eq. (6):

$$T_{f_i/f_j} = \frac{k_{f_i}{*}k_{f_j}}{k_{f_i}{*}d_{f_j} + k_{f_j}{*}d_{f_i}} {*} A_{f_if_j} \tag{6}$$

where, $A_{f_if_j}$ correspond to the exchange surface between the two homogenized grid cells, k_{f_i} and k_{f_j} correspond to the homogenized fractures permeabilities, respectively to node i and node j. The distances d_{f_j} and d_{f_j} correspond to the average distance from the center of the homogenized grid cell to the exchange surface.

2.5. Intra-matrix and tight matrix to homogenized fractures flow

The MINC proximity function (see; Farah (2016), Ricois et al. (2016)) is applied to compute the matrix and fracture exchange, and the connection between the subdivisions of the matrix (intra-matrix) media using the MINC proximity function is discussed.

Inside the SRV, a connection between the matrix domain and the fractures must be handled. The calculation of the exchange surface of all sorts of fractures intersecting (connected) with a grid cell is considered. In other words; hydraulic, stimulated and non-stimulated natural fractures are taken into account in order to apply the MINC proximity function for matrix-fracture exchange modelling (see; Fig. 6(c), (d) and (e)) which is in a strong difference with Jiang and

Younis (2016) and Yan et al. (2017). To do so, a number of points are randomly launched (see; Fig. 6(c)). Furthermore, the distance of each point to the nearest fracture is calculated. Fig. 6(d) represents an illustration of the different calculated distances taking into account the fracture network; where, different colors (blue, orange, grey, purple and black) represent the distance to the nearest fracture. Note that, the blue points represent the nearest distances to the fracture network, where the black represent the farthest ones. Thus, the matrix grid cell is subdivided (see, Fig. 6(e)) relatively based on the distance from the fractures by using this distance distribution function.

Let's consider the example presented in Fig. 6, the fracture volume V_1, for a given distance d_{m1}, consists in the first continuum (#1) of the MINC method concerning the matrix media, which is connected to the homogenized fracture cell using Eq. (7):

$$T_{f_i\,/\,M_{\#1}} = \frac{k_{f_i} * k_m}{k_m * d_{f_i} + k_{f_i} * d_{m_{\#1}}} * A_{F_i f_j} \approx \frac{k_m}{d_{m_{\#1}}} * A_{F_i f_j} \tag{7}$$

where, $A_{F_i f_j}$ corresponds to the surface exchange between fractures and matrix taking into account all sort of connected fractures within this grid cell, k_{f_i} is the permeability of homogenized fracture cell, d_{f_i} corresponds to the half average fracture aperture, k_m correspond to the matrix permeability and $d_{m_{\#1}}$ to the average distance from the first continuum (#1) of the matrix media.

The MINC proximity function is computed using a random approach. Usually, the sub-domains (matrix refinement) are constrained by a given percentage of the total volume, defined by the user which gives him flexibility in subdividing the sub-regions depending on fractures density and flow regime (see; Farah et al. (2016)). So, we can consider the volumes are known. Instead, we need to determine the distances which separate two matrix sub-domains. This is not a difficult task; however, the biggest challenge is to calculate the area of an interface between two matrix sub-domains. One of the originalities of this work relies on the way we compute the well-known MINC method using a "proximity function" formalism (distribution function). In fact, the information from our distance distribution function (Fig. 6(d)) is used in order: (1) to subdivide the matrix domain (Fig. 6(e)), (2) to calculate the average distances per matrix sub-domains to the fracture media and (3) to calculate the exchange surface between two consecutives matrix sub-domains.

In order to calculate the matrix-matrix interaction surface between two sub-domains, we suggest approximating this exchange surface with the derivative of the cumulative volume function with respect to the distance as described in Eq. (8):

$$A_{exchange_{i,i+1}} = \frac{dV}{dx} = \frac{V_{i+1} - V_{i-1}}{d_{i+1} - d_{i-1}} \tag{8}$$

where, the distance d_{i+1} corresponds to the average distance from volume V_{i+1} to the fractures and d_{i-1} is the average distance of V_{i-1}. The volumes V_{i-1} and V_{i+1} correspond to the cumulative volume of grid cells $i+1$ and $i-1$; respectively. Note that, the volumes and the average distances are calculated using the distance distribution function.

Once the exchange area is known, the connection transmissibility between the matrix subdivisions is calculated by Eq. (9).

$$T_{M_i\,/\,M_{i+1}} = \frac{k_m}{d_{i,i+1}} * A_{exchange_{i,i+1}};\ where,\ i = 1,2,\ \ldots,\ (n_{subdivision} - 1). \tag{9}$$

where, $d_{i,i+1}$ corresponds to the average distance between two successive matrix subdivisions and $n_{\text{subdivision}}$ corresponds to the number of matrix refinement.

On the other hand, another potential connection could occur between a SRV matrix media (MINC subdivision) and a non-SRV matrix media. So, transmissibility value must be calculated in order to model properly fluid flow on the SRV boundary. This calculation is not presented here, however for a detailed description; see, Farah (2016).

The algorithm above is one which transforms a 3D problem into a 1D. In effect, the very low permeability characteristic of the tight matrix, compared to the fractures, makes the main flow mechanism (except gravity) to be close to a diffusivity problem (fracture to matrix and vice-versa) governed by moving boundaries into the fracture system and into the matrix system during the transient period. This requires a sufficiently refined discretization, evolving through time, limiting numerical dispersion within acceptable cost. This diffusive mechanism is classically solved in 3D even if it depends only on the directional matrix permeability considered, the distance to the fracture and fluid properties. Our algorithm uses this to aggregate information in terms of distance to the closest fracture, thus 1D, using the so-called proximity functions. In addition, any directional anisotropy could be accounted for using a normalized distance (Delorme, 2015). McClure 2017 provides an example of reducing 3D into a 1D problem when dealing with leak-off term estimation. However, complex fracture geometries often found in unconventional reservoirs, construction of a mesh can be challenging and fastidious, especially in 3D. Our technique is useful because it avoids redoing the overall procedure. The proximity functions (and geometrical issues) are solved one time, not requiring conforming mesh, and can then be used in AMR technologies to restitute the accurate life periods field behavior. The main limitation is the vertical fluid flows, created by gravity for example. This is one of our current research interests. A possible way to include gravity would be to add in the equation a hydraulic head adjustment to the matrix pressure boundary condition in the 1D solution to the diffusivity equation. Another drawback is that the volume of the 1D matrix sub-element is higher than the 3D refined ones, increasing numerical dispersion. Yet, again, as fractures are more conductive, they favor equilibration at the boundaries of the problem, justifying this dilution into the matrix according to the distance to the fractures (such an effect is widely observed in connected fractured reservoir where the transition zone between water, oil and gas due to capillarity is absent).

2.6. Summary

This part sums up our DFM-MINC proximity function approach early proposed in this section. Fig. 7(a) and (b) present a 3D and 2D fracture view, respectively. Fig. 7(c) describes the principle behind our methodology which transforms a 3D problem (Fig. 7(a)) to a 1D one in conjunction with a limited number of node at each intersection of active fracture plane (a red node is assigned to such an intersection). Moreover, Fig. 7(c) illustrates the different possible connections occurring into a SRV grid cell where; hydraulic, natural stimulated, natural non-stimulated and isolated fractures exist. Connection can be classified as; Hydraulic (F) – Hydraulic (F), Hydraulic (F) – Homogenized (f), Homogenized (f) – Homogenized (f), Homogenized (f) – Matrix#1 (M_1) and finally Matrix – Matrix (for a MINC6 model, 6 matrix subdivisions exist; $M_1 - M_2 - M_3 - M_4 - M_5 - M_6$ are connected to each other's).

Our modelling approach is based on a triple continuum media, taking into consideration: (1) matrix media (m), (2) homogenized fracture media (f) and (3) highly conductive fractures (F), which are explicitly discretized. The MINC formalism is implemented to model flow exchange between the matrix media and the fractures (all the existing fractures).

Fig. 8(a), (b) and (c) present some of the advantages and disadvantages from the existing models in the literature. On the other hand, Fig. 8(d) summarizes the principle basic behind our proposed DFM-MINC proximity function by highlighting several advantages resulting from this proposed approach.

In summary, several advantages of our proposed DFM-MINC proximity function are:

1. First, the hierarchical method significantly reduces the number of nodes when compared to a standard DFM.
2. Second, the implementation of the MINC method insures an adequate flow modelling simply by calculating a better pressure

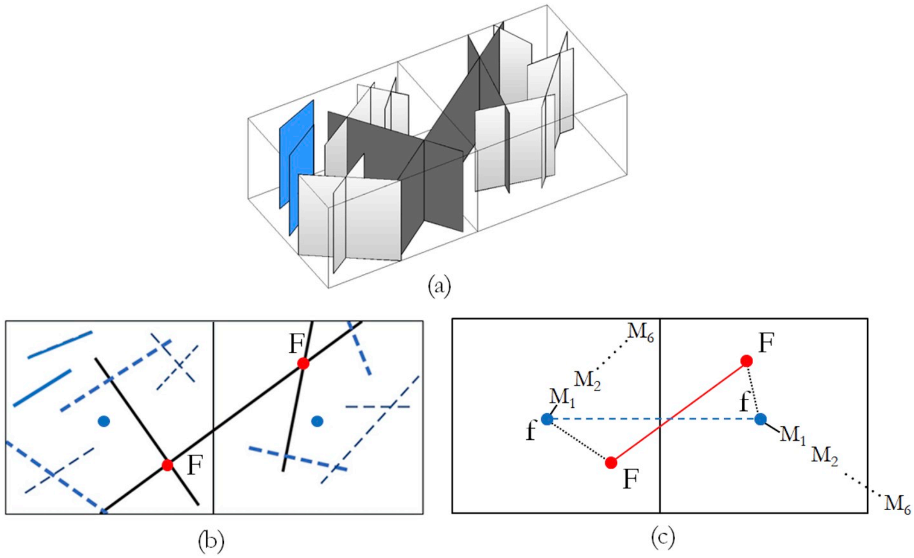

Fig. 7. Illustration of (a) a 3D fracture view, (b) a 2D fracture view and (c) the DFM-MINC proximity function optimization (1D problem) with the possible connection of the different media occurring between matrix (M_1, M_2 …, M_6), hydraulic fractures (F) and homogenized fractures (f).

gradient through the matrix domain.

3. Third, the 3D reservoir problem is simulated essentially by a series of a 1D flow problem numerically simpler.
4. Fourth, our DFM-MINC proximity function is meshless. In other words, the whole approach consists in a virtual mesh with nodes connected to each other, using transmissibility values mimicking flow exchange from matrix media through the discrete fracture network to the well.
5. Fifth, it should be mentioned that our approach has the advantages of reduced computational cost, while entirely bypassing the challenges in gridding the refined scale model. When identified, the primary fracture network may be discretized with a minimal number of nodes (a fracture node to each fractures plane intersection) and exchange terms have been explicitly described for embedding it in any reservoir grid with potential large grid cell sizes.
6. Last but not least, the user has the possibility to choose the Cartesian grid mesh in order to compute the MINC proximity function. Moreover, the user is able to fix the level of matrix refinement needed, which is a function of the fractures density and flow regime

Table 1
A summary of the existing connection and the related transmissibility formula used to connect different media.

Connection between media	Transmissibility
Well – Hydraulic fractures	$T_{Well\ /\ F} = \frac{k_F}{d_{well-F}} A_F$ and a PI to relate the wellbore pressure
Hydraulic - Hydraulic fractures	$T_{F_i\ /\ F_j} = \frac{k_F}{D_{ij}} A_F$, where $A_F = e_F{*}Z_F$
Hydraulic - Homogenized fractures	$T_{F_i\ /\ f_j} \approx \frac{k_{f_i}}{d_{f_i}}{*}A_{F_i}$
Homogenized - Hom. fractures	$T_{f_i\ /\ f_j} = \frac{k_{f_i}{*}k_{f_j}}{k_{f_i}{*}d_{f_j} + k_{f_j}{*}d_{f_i}}{*}A_{f_i f_j}$
Homogenized - Matrix#1	$T_{f_i\ /\ M\#1} \approx \frac{k_m}{d_{mat\#1}}{*}A_{F_i f_j}$
Matrix - Matrix (via MINC)	$T_{M_i\ /\ M_{i+1}} = \frac{k_m}{d_{i,i+1}}{*}A_{exchange_{i,i+1}}$

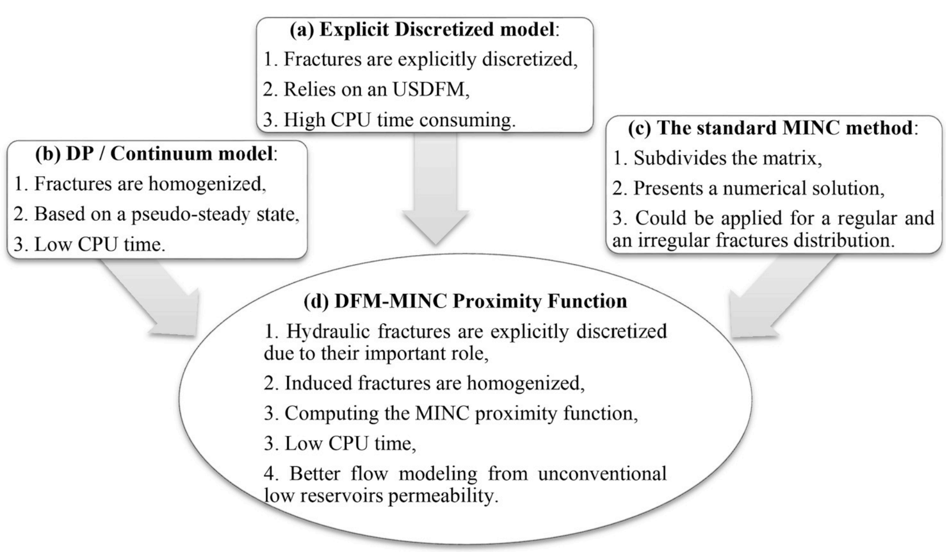

Fig. 8. The principle idea behind our triple continuum approach presenting: (a) the explicit discretized model, (b) the DP model and (c) the MINC method, leading to (d) our DFM-MINC proximity function for flow modelling from unconventional low reservoir permeability.

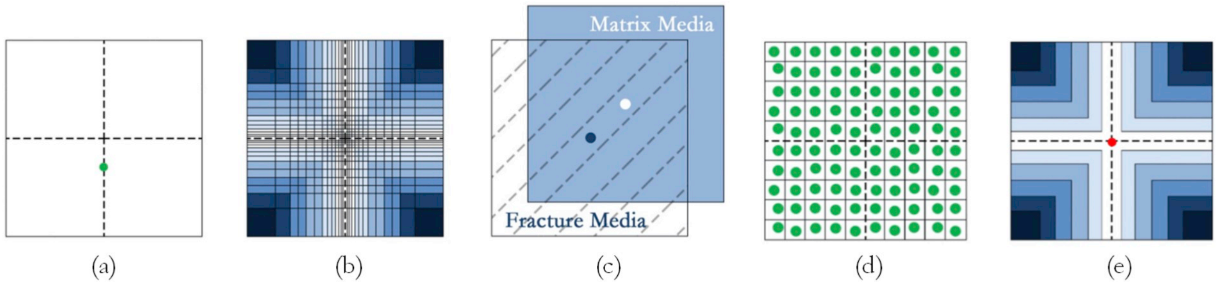

Fig. 9. Illustration of (a) a cross fracture model, (b) the explicit discretized model, (c) standard dual-porosity model, (d) the stochastic approach for a regular distribution of p points (p = 100), where the volume is discretized into p equal volume (cubic or rectangular) sub-domains and then a randomly point in each discretized domain is selected and (e) the optimization of the MINC proximity function.

(see; Farah et al. (2016)).

Table 1 summarizes the different possible connections occurring into our model. Besides, transmissibility calculations between existing media are presented. Note that, our proposed DFM-MINC proximity function is based on a triple medium, where six main transmissibility calculations are done in order to describe the flow behavior for such problem.

3. Validation of the DFM - cross fractures case

In this part, a simple case treating a single-phase flow is studied in order to validate the DFM. The following example consists in a matrix block of 65 ft in x and y directions with the presence of two hydraulic fractures with a fracture aperture fixed at 0.04 ft placed in the center of the block as shown in Fig. 9. The permeabilities are defined as 10^{-4} mD and 2000 mD, in the matrix and fracture media; respectively. The porosity of the matrix media is 0.05. The depth of the block is 330 ft in z direction. A horizontal well is placed into the formation. A horizontal well (green node in Fig. 9(a)) is placed and intersects with the hydraulic fracture (dashed line).

Three simulation models are performed and compared. First, an explicit model which discretized the fractures using a local grid refinement (LGR) technique around the fractures is taken into consideration. This model uses very small grid cells and is set as a reference solution (Fig. 9(b)). A standard dual-porosity (DP) model using a block of 65 ft is performed. Care was taken in the calculation of the effective fracture permeability and porosity for the DP model (Fig. 9(c)). On the other hand, in order to perform the MINC proximity function, p random points are launched (Fig. 9(d)) and our DFM is illustrated in Fig. 9(e), where a red dot is assigned to the intersection between the hydraulic fractures. Note that, our example is based on a MINC6 model.

Fig. 10(a) and (b) illustrate the cumulative distribution function for the example presented earlier in this section. Fig. 10(a) presents three samples of 100 points; Random #1, 2 and 3. Fig. 10(b) illustrates the cumulative distribution function for 1000 and 10,000 points. Clearly, increasing the number of random points increases the reliability of the distribution function leading to a better estimation of the exchange surface. In fact, as the number of randomly points increases, the precision of the transmissibility calculation increases as well, our DFM becoming more and more accurate in comparison to the reference solution. However, in practice we should limit the number of sampling points in due to CPU time constraint. Hereafter, the number of random points is limited at 100 points.

For this case gas is the fluid chosen. The initial reservoir pressure is 3800 psi and the bottom hole well flowing pressure is 1000 psi. The cumulative gas production resulting from different simulation models are presented in Fig. 10(c). Clearly, the DP model is not accurate comparing to the explicit discretized model. However, our DFM using three different point distributions presents accurate results in comparison to the reference solution. Based on the results shown in Fig. 9(c) we can conclude that our DFM is an improvement over the DP solution and that the MINC proximity function could handle the matrix-fracture exchange with a very good accuracy. More validating results have been investigated in Farah (2016); the reference solution, the dual porosity model and our DFM-MINC proximity function are there compared in many configurations such as; isolated fracture, orthogonal fractures, diagonal fractures and an irregular fractures distribution; all leading to our model validation.

4. Application to a synthetic 2D discrete fracture network

For this case, a more representative synthetic 2D case is considered, first using a single-phase gas reservoir and then a two-phase tight oil example. Different matrix permeability values are used; testing the robustness of the model when confronted to a multiphase flow problem, which makes the simulation quite challenging (see; Khvoenkova et al. (2015), Jiang and Younis (2017)). For a tight-oil reservoir example,

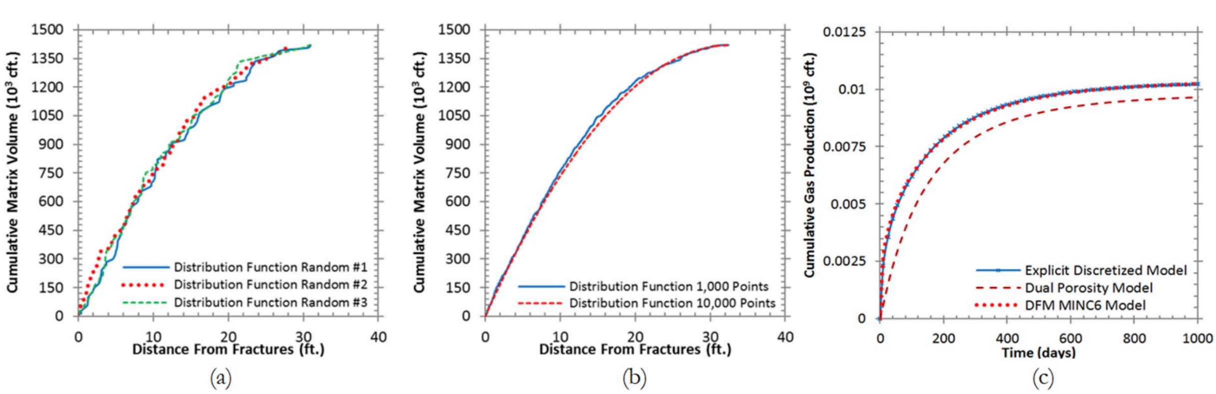

Fig. 10. Illustration of the cumulative distribution function for (a) a sample of 100 points and (b) 1000 points using the randomly discretized technique for the block of 50 ft and (c) the cumulative gas production for 1000 days of production.

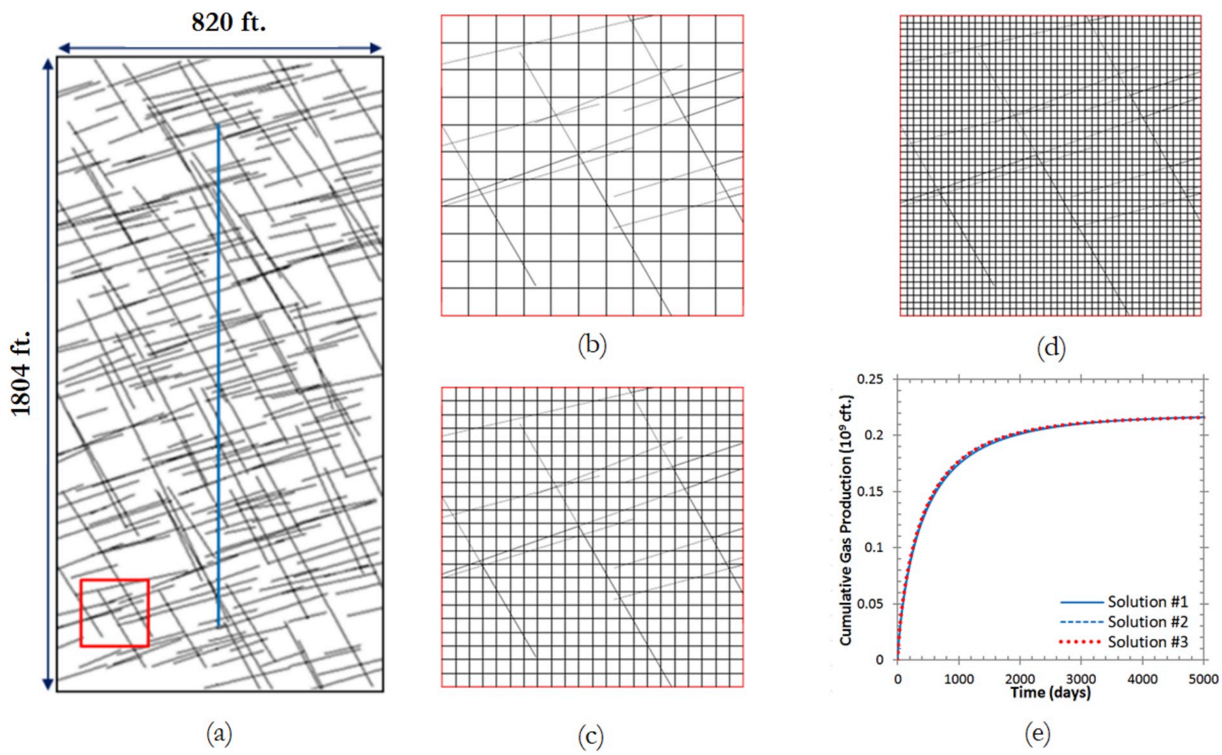

Fig. 11. Illustration of (a) the reservoir bounding box taking into account the DFN; (b) the grid refinement from the red box selected in Fig. 11(a) for Solution #1, (c) Solution #2, (d) Solution #3 and (e) the comparison of the cumulative gas production for the three solutions; Solution #1, #2 and #3. (For interpretation of the references to color in this figure legend, the reader is referred to the Web version of this article.)

when the fracture pressure drops below the bubble point, gas starts to appear in the matrix formation near the fracture faces. Standard approaches based on DP formulations cannot correctly handle this kind of problems. However, our proposed DFM-MINC proximity function is able to reproduce this behavior quite well.

The stimulated reservoir volume is at $820 \times 1804 \times 20\,ft^3$ as shown in Fig. 11(a). The reservoir parameters of the 2D example presented in Fig. 10(a) are summarized in Table 2. A horizontal well is placed in the x-direction and in the middle of the reservoir. The reservoir consists in 3 sets of 276 fractures (see, Fig. 11(a)). The hydraulic fracture (solid blue line in Fig. 11(a)) oriented in y-direction has a width of 0.012 ft and a permeability of 20 Darcy, while the two sets of stimulated natural fractures have a thickness varying from 0.004 ft to 0.005 ft and a permeability varying from 250 mD - 300 mD (An average of conductivity varying from 1 mD-ft to 1.5 mD-ft). The first set of natural fractures denoted Fracture set_1 is oriented with an average angle of 15° to the north and has a mean of 200 ft in length with a fracture density of 0.03. The second set of fractures denoted Fracture set_2 has an average orientation of 115° to the north and a mean length of 400 ft with a fracture density of 0.015. A conductivity criterion of 2 mD.ft is applied on the connected DFN. So, apart from the high conductive hydraulic fracture, all other fractures, including stimulated and non-stimulated natural fractures are homogenized inside the SRV (global homogenization and not Oda-type of up-scaling). Isolated fractures are not taken into consideration neither in computing the reference solution nor in our DFM. In fact, only a connected discrete fracture network is considered and studied. The hydraulic fracture is considered as a rectangular in a vertical plane with the half-length of 738 ft (total length of 1476 ft) in y-direction. The reservoir net thickness is 20 ft and the top of the reservoir is set at 3950 ft.

Table 2
Reservoir properties of the 2D synthetic example presented in Fig. 11(a).

Property/Parameter	Value	Unit
Hydraulic Fracture Permeability	20	D
Induced-fracture Permeability	300–400	mD
Hydraulic Fracture Width	0.012	ft
Induced-fracture Width	0.004–0.005	ft
Reservoir Net Thickness	20	ft
Top of the Reservoir	3950	ft

4.1. Generation of a reference solution

In order to provide a reference solution, the matrix media is discretized using very fine grid cells and the discrete fracture network is explicitly discretized taking into account all sort of connected fractures, where the matrix cells exchange with fracture nodes are estimated as described in Delorme et al. (2016). This approach consists in using our DFM-MINC proximity function of one single level (MINC1) with fine matrix cells volume.

To provide a reliable reference solution, three simulations consisting in three different mesh refinements are done, called Solution #1, #2 and #3 (see, Fig. 11(b), (c) and (d)). Fig. 11(b), (c) and (d) correspond to the red box selected in Fig. 11(a). The first (Solution #1) consists in 550000 grid cells. The second and the third consist in 2.2 and 8.8 million grid cells; respectively. In fact, the SRV has been discretized in x, y and z direction as following; 500×1100 x 1; 1000×2200 x 1 and 2000×4400 x 1 matrix grid cells, respectively for simulations #1, #2 and #3. Note that, the grid size is 1.64 ft in x and y direction for Solution #1, 0.82 ft for Solution #2 and 0.41 ft for Solution #3. Obviously, Solution #3 must be the most accurate one as it presents the smallest grid cell size comparing to Solution #1 and #2. In order to select to most reliable solution, the three solutions called Solution #1, #2 and #3 have been performed for a single-phase flow case taking a matrix permeability of $km = 10^{-4}$ mD. The results are illustrated in Fig. 11(e). Clearly, based on these results all solutions are very close comparing to each other. In particular, Solutions #2 and #3, with 2.2 and 8.8 million grid cells respectively, provide almost the same

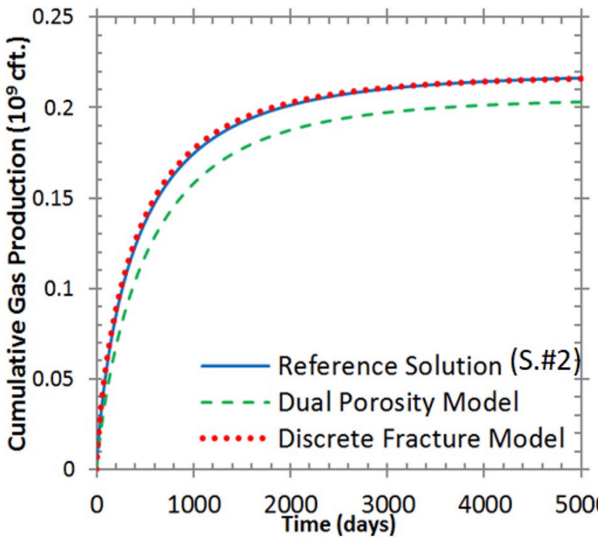

Fig. 12. Simulation results comparing the reference solution (Solution #2), dual-porosity model and the discrete fracture model for the shale-gas reservoir example.

results concerning the cumulative gas production after 5000 days of production. However, the CPU time of the Solution #1, #2 and #3 are 2 h, 6 h and 34 h, respectively. Due to a high CPU time presented by Solution #3; Solution #2 consisting in a 2.2 million grid cells can be reasonably considered as a reference solution. So in the following, Solution #2 is considered as a reference solution for single and multiphase flow simulations.

4.2. Shale-gas reservoir

For this study, only a single phase flow (gas only) is taken into account. Moreover, three simulation models, an explicit discretized model, a dual-porosity model and the DFM based on a MINC proximity function, are performed and compared. As mentioned above, the reference solution consists in 2.2 million grid cells. Also, it must be mentioned that the equivalent permeabilities of the DFM are computed with a global numerical upscaling method on the homogenized fracture cells.

The initial reservoir pressure and the bottom hole pressure are set at 3800 and 1000 psi respectively. The matrix permeability is 10^{-4} mD. Moreover, Fig. 12 presents the comparison of the reference solution (Solution #2), the dual-porosity model and the DFM for 5000 days of production. Clearly, based on our results from this case the DFM presents a better result than the dual-porosity model. Thus, the implementation of the MINC proximity function into the DFM improves significantly the capability to predict inter-porosity flow exchange. Based on these results, we conclude that our DFM is able to predict gas production from unconventional fractured shale-gas reservoirs and provides an accurate result comparing to a reference solution. Besides matching the reference solution, the DFM decreases greatly the CPU time. The DFM took only 20 s to perform the 2D synthetic shale-gas reservoirs for a single-phase flow problem, while it took around 6 h for the reference solution (Solution #2) to be performed. The proposed DFM proves then its efficiency.

4.3. Tight-oil reservoir

The next simulation scenario retains the same fracture network as presented earlier (see; Fig. 11(a)). In this section, we evaluate the accuracy and the ability of the model to treat a multiphase flow, where a tight-oil reservoir is studied. Initially, both oil and water are present in the reservoir. We consider the initial water saturation in this shale oil reservoir at 0.4, where the irreducible water saturation is set at 0.1. Also, the formation porosity is 0.05. The matrix permeability is set as 10^{-4} mD. The initial reservoir pressure is 3800 psi and the horizontal well produces at a constant bottom hole pressure of 1160 psi, which is below the bubble point pressure set as 2710 psi. The top of the reservoir is 3950 ft. Fig. 13(a),(b), (c) and (d) illustrate the relative permeabilities curves and capillary pressure for the matrix media, for the oil-water system and the gas-oil system; respectively.

Once the well is put into production, the reservoir pressure begins to decrease and when the reservoir pressure decreases below the bubble point pressure, gas starts to appear inside the reservoir near fracture faces. The bubble point distance to the fracture will move during the production. Such phenomenon is difficult to reproduce with a dual-porosity model because of the large and heterogeneous block occurring in very low matrix permeability. Especially during the transient period where a non-linear variation of the pressure in the matrix media renders difficult the estimation of the pseudo matrix pressure average. However, the MINC method presents a solution for this problem.

Simulations results are presented in Fig. 14. Our DFM, based on different MINC model (MINC2, MINC4 and MINC8), is compared to the reference solution. Fig. 14(a), (b), (c), (d) and (e) show respectively the results of daily gas rate, daily oil rate, cumulative gas production, cumulative oil production and the gas oil ratio (GOR). Fig. 14(a) and (b) illustrate the daily gas and oil rate after 2000 days of production for the three simulation models whereas Fig. 14(c) and (d) show the cumulative gas and oil production for 5000 days of production. Clearly, the DFM based on a MINC8 model (dotted red line) matches the reference solution, predicting the same amount of cumulative gas production (around $30*10^6$ cft) after 5000 days. As well as for the cumulative oil production, our DFM predicts around 14000 bbl where the reference solution predicts around 13500 bbl at the end of production. Fig. 14(e) illustrates the GOR for 5000 days. Our DFM based on a MINC8 model shows the same trend as the reference solution. We should also notice that the grid size (depending there on the MINC refinement) impact the predictions (same conclusions were given by Chai et al. (2016)), appealing adapted meshing strategies.

Fig. 15 shows a comparison of the tight-oil reservoir simulations for different matrix permeability $k_m = 10^{-4}$ mD and $k_m = 10^{-5}$ mD,

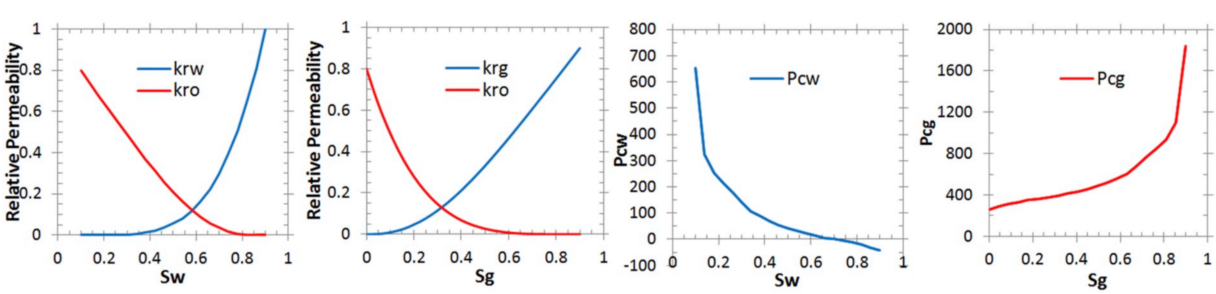

Fig. 13. (a) Water/oil and (b) gas/oil relative permeability curves, (c) Water/oil and (d) gas/oil capillary pressures.

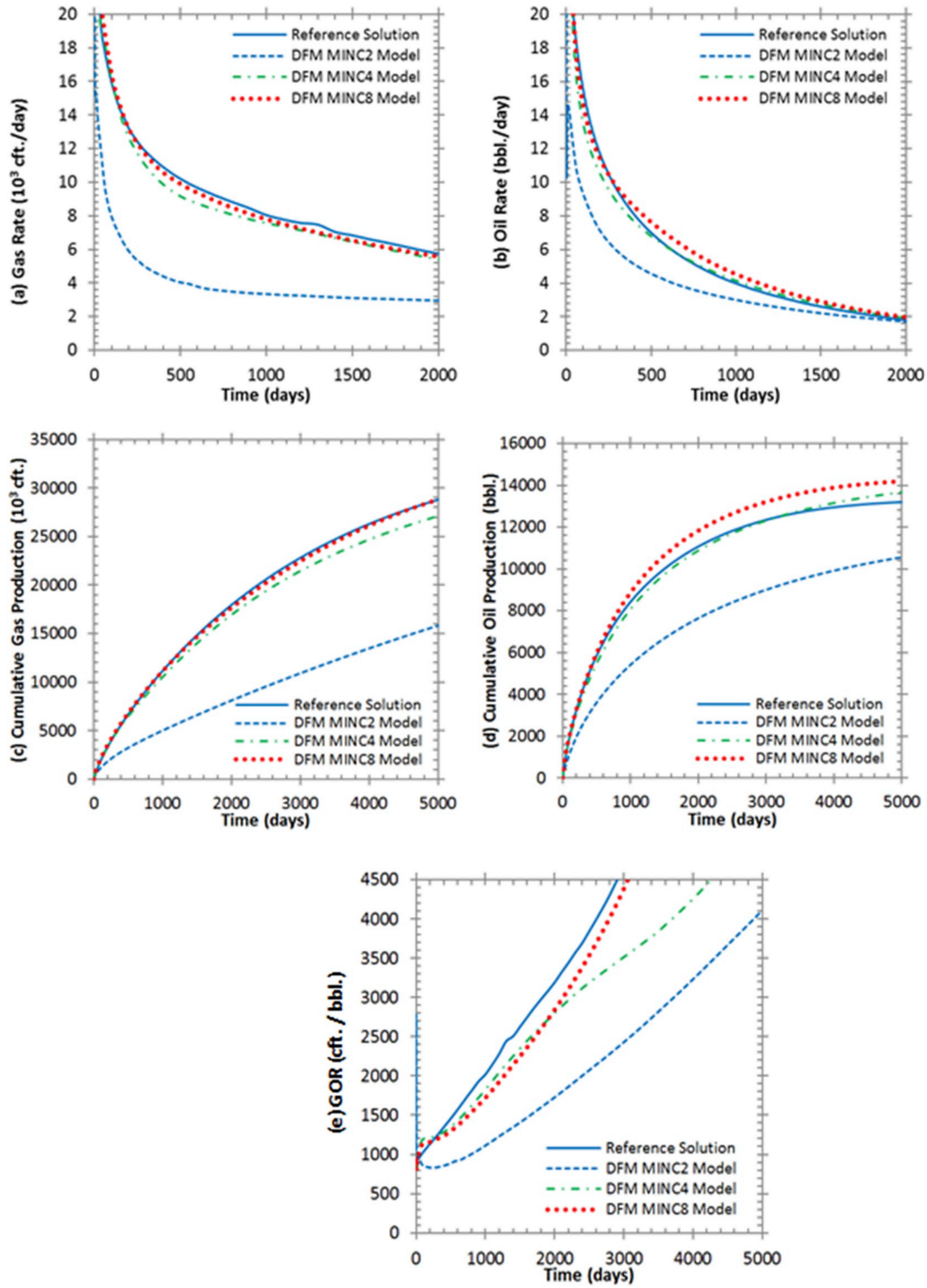

Fig. 14. (a) Simulation results of the tight-oil reservoir with km = 10-4 mD (a) gas rate, (b) oil rate, (c) the cumulative gas production, (d) the cumulative oil production and (e) the GOR.

testing the DFM to different matrix permeability. Based on results, our DFM is able to reasonably match flow production (more so for the lower permeability), as well as the GOR, for which trends are equally good for both permeabilities. Based on results from Fig. 15, our DFM proved it is ability to predict flow production for different matrix permeability for a multiphase flow problem. Moreover, our DFM reduces enormously the CPU time from 7 h to 30 s simply by reducing the number of grid cells from 2,200,624 to 387 grid cells.

Finally, results from all cases (Figs. 12, Figs. 14 and 15) show good prediction for both single and multi-phase production in shale-gas or tight-oil reservoirs. Computing the MINC method using the proximity function stochastic process is an efficient method to simulate flow for fractured reservoirs, enabling a correct GOR prediction, which is difficult in low-permeability multiphase flow unconventional reservoirs. Although the DFM approach was introduced to simulate shale-gas reservoirs, it also showed its ability to properly model a tight-oil reservoir example.

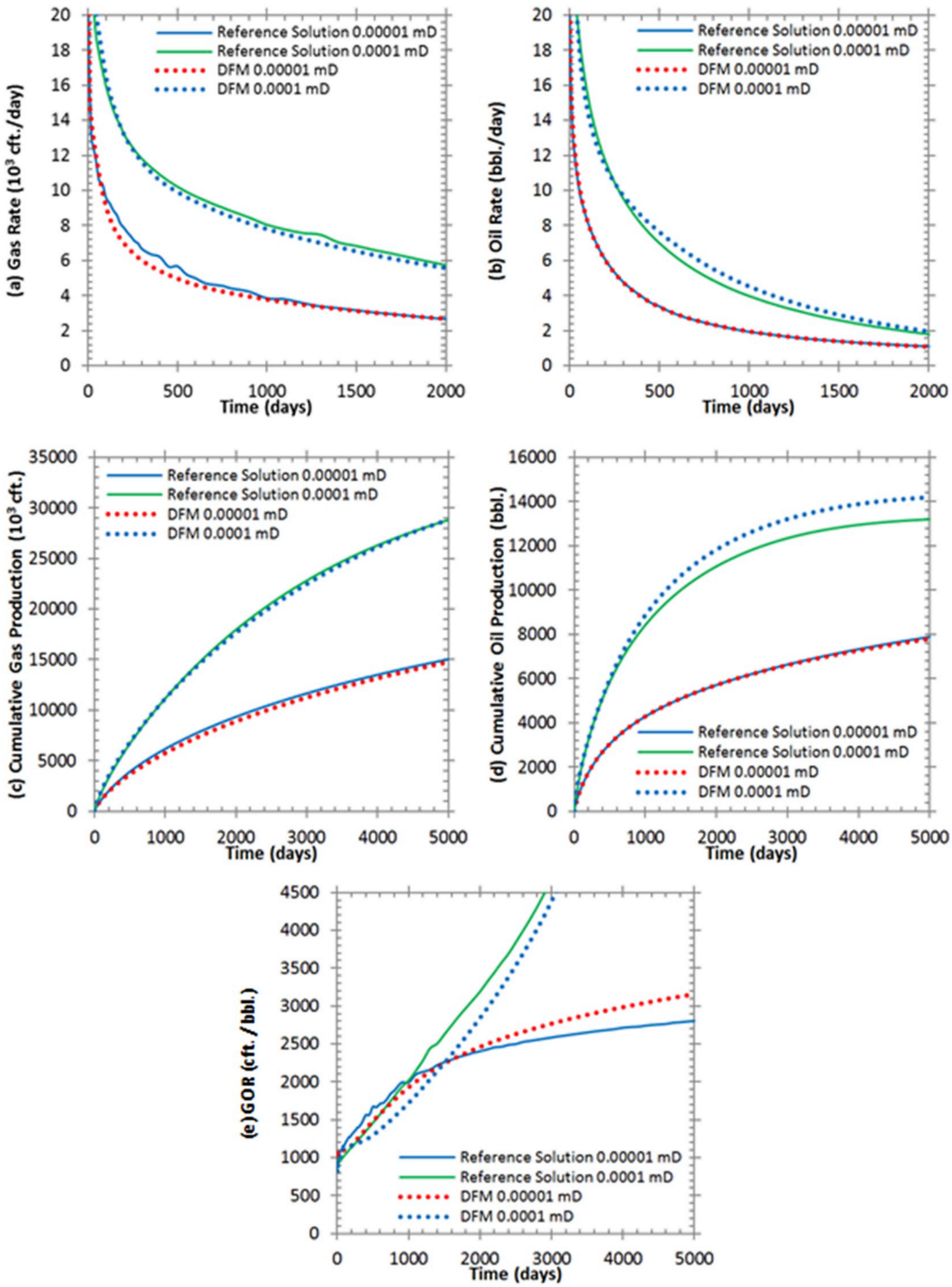

Fig. 15. Comparison of the simulation results between the reference solution and our DFM of the tight-oil reservoir for km = 10^{-4} mD and km = 10^{-5} mD (a) gas rate, (b) oil rate, (c) the cumulative gas production, (d) the cumulative oil production and (e) the gas oil ratio (GOR).

5. Conclusions

This paper presents a practical hybrid methodology based on a MINC proximity function in order to model flow behavior from low permeable fractured reservoirs. The method combines the advantages of multi-continuum and Discrete Fracture Model representations for fractured unconventional reservoir simulation. It is specifically appropriate for large reservoir modelling and interferences testing analysis or when data are sparse to perform sensitivity studies. Through this work, the reliability and the ability of this proposed DFM-MINC proximity function is tested on an irregular complex fracture network, including an irregular fracture distribution for a multiphase flow with a low reservoir permeability of 0.0001 mD and 0.00001 mD.

Clearly, based on our approach we aim at preserving the continuum-type model advantages while explicitly addressing the role of dominant stimulated fractures as main fluid conduits connecting the reservoir to the wellbore. We conclude the following:

1. Realistic (potentially) complex fracture geometry can be represented; the hypotheses used to simplify the model are accurate to

reproduce refined scale simulations.

2. Severe permeability contrasts that characterize tight-oil/shale gas reservoirs are adequately captured using both overlapping fracture and matrix porous media. The MINC proximity function can easily handle such phenomenon due to the very small nested matrix sub-cells near fractures faces.
3. Computational cost to model stimulated systems can be reduced using this hybrid methodology derived from MINC concept. The 3D problem in the low permeable matrix is indeed reduced to a 1D problem in that case, reducing the required number of unknowns to efficiently capture transient effects.
4. 3D proximity functions can be easily calculated and implemented in any reservoir simulators through an option of non-neighbor connections, offering flexibility. It can be inserted in practical integrated studies either to adjust numerical parameters or to perform sensitivity analysis.

A critical remaining step for fulfilling this kind of modelling is to parameterize the criterion establishing the different levels of media as well as the type and number of refinement to use within the proximity function. These issues have been partially addressed in this work. It is suggested that the criterion for classification should be able to identify the primary fractures that exhibit significant potential gradient and have a large impact on the transient flow regime during production process. Sensitivity on the cell sizes to use inside a given data-set would also provide some highlights helping the user to make the best decision based on his objectives.

Finally, the results from the presented applications are good enough to compare with a reference solution (obtaining similar results with a gain of an order of magnitude of 4 in CPU time), while a standard DP model is not accurate at all. The large CPU gain and precise proximity functions evaluation of the presented model should allow to deeply study other involved mechanisms (currently neglected even if it could be important in precise cases) such as Fick diffusion (Yan et al. (2016b)) or interactions with vuggs (Zhang et al. (2018)). The formalism of these models is indeed very close to our approach. Moreover, the applicability, ability, efficiency, and robustness of the proposed DFM to model flow behavior from low permeable fractured reservoirs is proven through the examples presented in this work, which provide accurate simulation results for both single and multiphase flow problems. Furthermore, our DFM is particularly useful for multi-phase flow reservoir simulations.

Acknowledgements

The authors gratefully acknowledge IFP Energies nouvelles for their support and the helpful reviewers' comments.

Appendix A. Supplementary data

Supplementary data to this article can be found online at https://doi.org/10.1016/j.petrol.2018.10.014.

References

Akkutlu, I.Y., Efendiev, Y., Vasilyeva, M., Wang, Y., 2017. Multiscale model reduction for shale gas transport in a coupled discrete fracture and dual-continuum porous media. J. Nat. Gas Sci. Eng. 48, 65–76.

Al-Rbeawi, S., 2017. How much stimulated reservoir volume and induced matrix permeability could enhance unconventional reservoir performance. J. Nat. Gas Sci. Eng. 46, 764–781. https://doi.org/10.1016/j.jngse.2017.08.017.

Al-Rbeawi, S., 2018. Bivariate Log-Normal Distribution of Stimulated Matrix Permeability and Block Size in Fractured Reservoirs: Proposing New Multilinear-flow Regime for Transient-state Production. paper SPE-189993-PA. https://doi.org/10.2118/189993-PA.

Arps, J.J., 1945. Analysis of decline curves. Trans. AIME 160, 228–247. https://doi.org/10.2118/945228-G.

Artus, V., Fructus, D., 2012. Transmissibility corrections and grid control for shale gas numerical production forecasts. Oil & Gas Sci. Tech.–Revue d'IFP Energies nouvelles 67 (5), 805–821. https://doi.org/10.2516/ogst/2012054.

Barree, R.D., 1983. A practical numerical simulator for three-dimensional fracture propagation in heterogeneous media. SPE Reservoir Simulation Symposium. Society of Petroleum Engineers. https://doi.org/10.2118/12273-MS.

Berrone, S., Fidelibus, C., Pieraccini, S., Scialo, S., 2014. Simulation of the steady-state flow in discrete fracture networks with non-conforming meshes and extended finite elements. Rock Mech. Rock Eng. 47 (6), 2171–2182. https://doi.org/10.1007/s00603-013-0513-5.

Bouteca, M.J., 1988. Hydraulic Fracturing Model Based on a Three-dimensional Closed Form: Tests and Analysis of Fracture Geometry and Containment. Society of Petroleum Engineers. https://doi.org/10.2118/16432-PA.

Chai, Z., Yan, B., Killough, J.E., Wang, Y., 2016, November. Dynamic embedded discrete fracture multi-continuum model for the simulation of fractured shale reservoirs. In: International Petroleum Technology Conference, . https://doi.org/10.2523/IPTC-18887-MS.

Clarkson, C.R., 2013. Production data analysis of unconventional gas wells: review of theory and best practices. Int. J. Coal Geol. 109–110, 101–146. https://doi.org/10.1016/j.coal.2013.01.002.

Daneshy, A., 1973. On the design of vertical hydraulic fractures. J. Petrol. Technol. 25 (01), 83–97. SPE-3654-PA. https://doi.org/10.2118/3654-PA.

Delorme, M., 2015. Ecoulements en milieux fracturés: vers une intégration des méthodes discrètes et continues. Ph.D. http://ethesis.inp-toulouse.fr/archive/00003021/.

Delorme, M., Daniel, J.-M., Kada-Kloucha, C., Khvoenkova, N., Schueller, S., Souque, C., 2013. An efficient model to simulate reservoir stimulation and induced microseismic events on 3D discrete fracture network for unconventional reservoirs. Unconventional Res. Tech. Conf. https://doi.org/10.1190/urtec2013-146.

Delorme, M., Bossie-Codreanu, D., Ben-Gharbia, I., Khebzegga, O., Khebzegga, N., Ricois, O.M., 2016, June 1. Unconventional Production Forecast Needs Integration of Field Hydraulic Stimulation Data through Fracture Model Calibration and Optimized Numerical Scheme. Society of Petroleum Engineershttps://doi.org/10.2118/180946-MS.

Delorme, M., Bossie-Codreanu, D., Khvoenkova, N., 2017, May 15. Improved Data Characterization and Integration for Better Hydraulic Fracturing Design Prediction. Geoconvention 2017 Calgary.

Elmo, D., Stead, D., 2010. An integrated numerical modelling–discrete fracture network approach applied to the characterization of rock mass strength of naturally fractured pillars. Rock Mech. Rock Eng. 43, 3. https://doi.org/10.1007/s00603-009-0027-3.

Farah, N., 2016. Flow Modelling in Low Permeability Unconventional Reservoirs. Ph.D. IFP Energies nouvelles, Presented at UPMC, Paris VI, Paris, France December 6th. https://tel.archives-ouvertes.fr/tel-01526386.

Farah, N., Ding, D.Y., Wu, Y.S., 2016. Simulation of the impact of fracturing fluid induced formation damage in shale gas reservoirs. SPE J. Reservoir Eval. Eng. https://doi.org/10.2118/173264-PA.

Fetkovich, M.J., Fetkovich, E.J., Fetkovich, M.D., 1996. Useful concepts for decline curve forecasting, reserve estimation, and analysis. SPE Reservoir Eng. 11 (01), 13–22. paper SPE-28628-PA. https://doi.org/10.2118/28628-PA.

Fuentes-Cruz, G., Gildin, E., Valko, P.P., 2014. Analyzing Production Data from Hydraulically Fractured Wells: the Concept of Induced Permeability Field. paper SPE-163843-PA. https://doi.org/10.2118/163843-PA.

Fumagalli, A., Scotti, A., 2013. A numerical method for two-phase flow in fractured porous media with non-matching grids. Adv. Water Resour. 62, 454–464. https://doi.org/10.1016/j.advwatres.2013.04.001.

Huang, J., Safari, R., Lakshminarayanan, S., Mutlu, U., McClure, M., 2014. Impact of discrete fracture network (DFN) reactivation on productive stimulated rock volume: microseismic, geomechanics and reservoir coupling. In: Presented at: 48th US Rock Mechanics/Geomechanics Symposium, At Minneapolis, MN.

Jiang, J., Younis, R.M., 2016. Hybrid coupled discrete-fracture/matrix and multi-continuum models for unconventional-reservoir simulation. SPE J SPE-178430-PA. https://doi.org/10.2118/178430-PA.

Jiang, J., Younis, R.M., 2017. An improved projection-based embedded discrete fracture model (pEDFM) for multiphase flow in fractured reservoirs. Adv. Water Resour. 109, 267–289. https://doi.org/10.1016/j.advwatres.2017.09.017.

Karimi-Fard, M., Durlofsky, L.J., Aziz, K., 2004. An efficient discrete-fracture model applicable for general purpose reservoir simulators. SPE J. 9, 227–236. SPE-79699-MS. https://doi.org/10.2118/79699-MS.

Karimi-Fard, M., Gong, B., Durlofsky, L.J., 2006. Generation of Coarse-scale Continuum Flow Models from Detailed Fracture Characterizations. Department of Energy Resources Engineering, Stanford University, California, USA. https://doi.org/10.1029/2006WR005015.

Ketineni, S.P., Ertekin, T., 2012. January). Analysis of production decline characteristics of a multistage hydraulically fractured horizontal well in a naturally fractured reservoir. In: SPE Eastern Regional Meeting. Society of Petroleum Engineers SPE-161016-MS. https://doi.org/10.2118/161016-MS.

Khvoenkova, N., Delorme, M., 2009. Performance analysis of the hybrid fracture media upscaling approach on a realistic case of naturally fractured reservoir. In: International Petroleum Technology Conference, vol. 5. Society of Petroleum Engineers, pp. 3052–3061.

Khvoenkova, N., Delorme, M., 2011. An optimal method to model transient flows in 3D discrete fracture network. In: IAMG Conference, vol. 2011. pp. 1238–1249. https://doi.org/10.5242/iamg.2011.0088.

Khvoenkova, N., and Delorme, M., (2013). Method for generating a fractured reservoir mesh with a limited number of nodes in the matrix medium, U.S. Patent Application No. 13/644,479.

Khvoenkova, N., Bossie-Codreanu, D., Broussard, N., Delorme, M., Lecomte, J.C., 2015, September 28. Application of the DDFN (Discrete and Deformable Fracture Network) Method within an Integrated Unconventional Reservoir Study Workflow. Society of

Petroleum Engineershttps://doi.org/10.2118/175112-MS.
Kuchuk, F., Biryukov, D., 2014. Pressure-transient behavior of continuously and discretely fractured reservoirs. SPE Reservoir Eval. Eng. 17 (01), 82–97. SPE-158096-PA. https://doi.org/10.2118/158096-PA.
Lee, S.H., Lough, M.F., Jensen, C.L., 2001. Hierarchical modelling of flow in naturally fractured formations with multiple length scale. Water Resour. Res. 37 (3), 443–445. https://doi.org/10.1029/2000WR900340.
Mattar, L., Anderson, D.M., 2003. January). A systematic and comprehensive methodology for advanced analysis of production data. In: SPE Annual Technical Conference and Exhibition. Society of Petroleum Engineers SPE-84472-MS. https://doi.org/10.2118/84472-MS.
Mayerhofer, M.J., Lolon, E.P., Youngblood, J.E., Heinze, J.R., 2006. Integration of microseismic-fracture-mapping results with numerical fracture network production modelling in the Barnett Shale. In: SPE Annual Technical Conference and Exhibition, SPE-102103-MS. https://doi.org/10.2118/102103-MS.
McClure, M., 2017. An Accurate and Efficient Method for Calculating Fluid Exchange between Fractures and Matrix with a Non-conforming Mesh. arXiv preprint arXiv:1709.02493 [physics.geo-ph].
McClure, M., Babazadeh, M., Shiozawa, S., Huang, J., 2015. Fully coupled hydro-mechanical simulation of hydraulic fracturing in three-dimensional discrete fracture networks. In: SPE Hydraulic Fracturing Technology Conference, SPE-173354-MS. https://doi.org/10.2118/173354-MS.
Meyer, B.R., Bazan, L.W., 2011. A discrete fracture network model for hydraulically induced fractures-theory, parametric and case studies. In: SPE Hydraulic Fracturing Technology Conference, Paper SPE 140514.
Mi, L., Yan, B., Jiang, H., An, C., Wang, Y., Killough, J.E., 2017. An Enhanced Discrete Fracture Network model to simulate complex fracture distribution. J. Petrol. Sci. Eng. 156, 484–496. https://doi.org/10.1016/j.petrol.2017.06.035.
Moinfar, A., Narr, W., Hui, M.H., Mallison, B.T., Lee, S.H., 2011. Comparison of discrete-fracture and dual-permeability models for multiphase flow in naturally fractured reservoirs. In: SPE Reservoir Simulation Symposium, SPE-142295-MS. https://doi.org/10.2118/142295-MS.
Moinfar, A., Varavei, A., Sepehrnoori, K., Johns, R.T., 2013. Development of a coupled dual continuum and discrete fracture model for the simulation of unconventional reservoirs. In: SPE Reservoir Simulation Symposium. Society of Petroleum Engineers SPE-163647-MS. https://doi.org/10.2118/163647-MS.
Nagel, N.B., Sanchez-Nagel, M.A., Zhang, F., Garcia, X., Lee, B., 2013. Coupled numerical evaluations of the geomechanical interactions between a hydraulic fracture stimulation and a natural fracture system in shale formations. Rock Mech. Rock Eng. 46 (2013), 581. https://doi.org/10.1007/s00603-013-0391-x.
Ngo, T.D., Fourno, A., Noetinger, B., 2017. Modelling of transport processes through large-scale discrete fracture networks using conforming meshes and open-source software. J. Hydrol. 554, 66–79.
Norbeck, J., Huang, H., Podgorney, R., Horne, R., 2014. An Integrate Discrete Fracture Model for Description of Dynamic Behavior in Fractured Reservoirs. Department of Energy Resources Engineering, Stanford University, California, USA February 24-26, SGP-TR-202.
Nordgren, R.P., 1972. Propagation of a vertical hydraulic fracture. Soc. Petrol. Eng. J. 12 (04), 306–314. SPE-3009-PA. https://doi.org/10.2118/3009-PA.
Okouma Mangha, V., Ilk, D., Blasingame, T.A., Symmons, D., Hosseinpour-zonoozi, N., 2012. Practical considerations for decline curve analysis in unconventional reservoirs - application of recently developed rate-time relations. In: SPE Hydrocarbon Economics and Evaluation Symposium, paper SPE-162910-MS. https://doi.org/10.2118/162910-MS.
Ozkan, E., Brown, M.L., Raghavan, R., Kazemi, H., 2011. Comparison of fractured-horizontal-well performance in tight sand and shale reservoirs. SPE Reser. Eval. Eng. 14 (2), 248–259. https://doi.org/10.2118/121290-PA.
Parsegov, S.G., Niu, G., Schechter, D.S., Laprea-Bigott, M., 2018. Benefits of engineering fracture design. Lessons learned from underperformers in the midland basin. In: SPE Hydraulic Fracturing Technology Conference and Exhibition, paper SPE-189859-MS. https://doi.org/10.2118/189859-MS.
Pichot, G., Erhel, J., de Dreuzy, J.R., 2012. A generalized mixed hybrid mortar method for solving flow in stochastic discrete fracture networks. SIAM J. Sci. Comput. 34 (1), B86–B105. https://doi.org/10.1137/100804383.
Pruess, K., Karasaki, K., 1982. Proximity functions for modelling fluid and heat flow in reservoirs with stochastic fracture distributions. In: Submitted to the Stanford Geothermal Reservoir Engineering Workshop, December 14-16.
Raterman, K.T., Farrell, H.E., Mora, O.S., Janssen, A.L., Gomez, G.A., Busetti, S., Reid, R., 2017. Sampling a Stimulated Rock Volume: an Eagle Ford Example. Unconventional Resources Technology Conference URTeC 2670034.
Reichenberger, V., Jakobs, H., Bastian, P., Helmig, R., 2006. A mixed-dimensional finite volume method for two-phase flow in fractured porous media. Adv. Water Resour. 29 (7), 1020–1036.
Ricois, O.M., Gratien, J., BossieCodreanu, D., Khvoenkova, N., Delorme, M., 2016. Advantages of an unstructured unconventional fractured media model integrated within a multiphysics computational platform. In: International Petroleum Technology Conference, IPTC-18846-MS, . https://doi.org/10.2523/IPTC-18846-MS.
Sarda, S., Jeannin, L., Basquet, R., Bourbiaux, B., 2002. Hydraulic characterization of fractured reservoirs: simulation on discrete fracture models. SPE Reservoir Eval. Eng. 5 (2), 154–162. paper SPE-77300-PA. https://doi.org/10.2118/77300-PA.
Stalgorova, K., Mattar, L., 2013. Analytical model for unconventional multifractured composite systems. SPE Reservoir Eval. Eng. 16 (03), 246–256. SPE-162516-PA. https://doi.org/10.2118/162516-PA.
Sun, J., Schechter, D., 2015. Optimization-based unstructured meshing algorithms for simulation of hydraulically and naturally fractured reservoirs with variable distribution of fracture aperture, spacing, length and strike. SPE Reservoir Eval. Eng. 18 (04), 463–480. https://doi.org/10.13140/2.1.2999.8884.
Sun, J., Schechter, D., Huang, C.K., 2016. Grid-sensitivity Analysis and Comparison between Unstructured Perpendicular Bisector and Structured Tartan/local-grid-refinement Grids for Hydraulically Fractured Horizontal Wells in Eagle Ford Formation with Complicated Natural Fractures. paper SPE-177480-PA. https://doi.org/10.2118/177480-PA.
Weng, X., Kresse, O., Cohen, C.E., Wu, R., Gu, H., 2011. Modelling of hydraulic-fracture-network propagation in a naturally fractured formation. SPE Prod. Oper. 26 (04), 368–380. SPE-140253-PA. https://doi.org/10.2118/140253-PA.
Williams-Stroud, S., 2008. Using microseismic events to constrain fracture network models and implications for generating fracture flow properties for reservoir simulation. In: SPE Shale Gas Production Conference, Paper SPE-119895-MS, . https://doi.org/10.2118/119895-MS.
Wu, Y.S., Pruess, K., 1988. A multiple-porosity method for simulation of naturally fractured petroleum reservoirs. SPE Reservoir Eng. 3, 327–336. paper SPE-15129-PA. https://doi.org/10.2118/15129-PA.
Xu, W., Thiercelin, M.J., Ganguly, U., Weng, X., Gu, H., Onda, H., Le Calvez, J., 2010. Wiremesh: a novel shale fracturing simulator. In: International Oil and Gas Conference and Exhibition in China, Paper SPE-132218-MS, . https://doi.org/10.2118/132218-MS.
Yan, B., Alfi, M., An, C., Cao, Y., Wang, Y., Killough, J.E., 2016a. General Multi-Porosity simulation for fractured reservoir modelling. J. Nat. Gas Sci. Eng. 33, 777–791. https://doi.org/10.1016/j.jngse.2016.06.016.
Yan, B., Wang, Y., Killough, J.E., 2016b. Beyond dual-porosity modelling for the simulation of complex flow mechanisms in shale reservoirs. Comput. Geosci. 20 (1), 69–91. https://doi.org/10.2118/163651-MS.
Yan, B., Mi, L., Chai, Z., Wang, Y., Killough, J.E., 2017. An Enhanced Discrete Fracture Network model for multiphase flow in fractured reservoirs. J. Petrol. Sci. Eng. https://doi.org/10.1016/j.petrol.2017.12.016.
Yang, C., King, M.J., Datta-Gupta, A., 2017. Rapid Simulation of Naturally Fractured Unconventional Reservoirs with Unstructured Grids Using the Fast Marching Method. Society of Petroleum Engineershttps://doi.org/10.2118/182612-MS.
Zhang, N., Wang, Y., Sun, Q., Wang, Y., 2018. Multiscale mass transfer coupling of triple-continuum and discrete fractures for flow simulation in fractured vuggy porous media. Int. J. Heat Mass Tran. 116, 484–495. https://doi.org/10.1016/j.ijheatmasstransfer.2017.09.046.